

# Sorting method to extend the dynamic range of the Shack–Hartmann wave-front sensor

Junwon Lee, Roland V. Shack, and Michael R. Descour

We propose a simple and powerful algorithm to extend the dynamic range of a Shack–Hartmann wave-front sensor. In a conventional Shack–Hartmann wave-front sensor the dynamic range is limited by the  $f$ -number of a lenslet, because the focal spot is required to remain in the area confined by the single lenslet. The sorting method proposed here eliminates such a limitation and extends the dynamic range by tagging each spot in a special sequence. Since the sorting method is a simple algorithm that does not change the measurement configuration, there is no requirement for extra hardware, multiple measurements, or complicated algorithms. We not only present the theory and a calculation example of the sorting method but also actually implement measurement of a highly aberrated wave front from nonrotational symmetric optics. © 2005 Optical Society of America

*OCIS codes:* 120.3940, 350.4800.

## 1. Introduction

The Shack–Hartmann wave-front sensor has been a popular wave-front sensing instrument in various areas such as optical testing, astronomical adaptive optics, and ophthalmology since its invention.<sup>1–6</sup> The advantages of the Shack–Hartmann wave-front sensor are the simplicity of the configuration, real-time data processing, and a high dynamic range. In principle the Shack–Hartmann wave-front sensor samples a wave-front slope at a number of positions through measurement of the displacement of the focal spots created by a lenslet array. The original wave front is reconstructed, based on the wave-front slope data, by using well-known mathematical tools.<sup>7–14</sup> Mathematically the wave-front reconstruction is equivalent to solving a linear inverse problem.

In a conventional Shack–Hartmann wave-front sensor the focal spot is required to remain in the image area confined by a lenslet, so that the dynamic range (the maximum tolerable spot displacement) of the Shack–Hartmann wave-front sensor is limited by

the  $f$ -number of the lenslet.<sup>15</sup> It is well known that there is a trade-off between the sensitivity and the dynamic range of the Shack–Hartmann wave-front sensor. If the  $f$ -number is relatively short, a high dynamic range is achieved, but the corresponding sensitivity is degraded and vice versa. A novel approach is necessary to overcome the trade-off in a conventional Shack–Hartmann wave-front sensor.

The earliest approach to overcoming the trade-off is to track the movement of focal spots along an optical axis by measurements at additional planes between a lenslet array and a detection plane, usually the focal plane of the lenslet.<sup>16</sup> Another novel approach is to use a modified unwrapping algorithm to eliminate the discontinuities in the patterns of the local positions, which are wrapped modulo  $P$ , where  $P$  is the pitch of a single lenslet.<sup>15</sup> The technique presented in Ref. 17 uses two different measurements, including a conventional image of the wave front and the use of the classical Shack–Hartmann sensor image. In Ref. 18 an estimate of the positions of the focal spots of neighboring lenslets is proposed by extrapolating a two-dimensional spline function that assigns the spots to their respective reference points.

There are other approaches that use specially designed devices. For example, an astigmatic lenslet array that gives a kind of mark to each spot that does not affect the position of the center of the spot but that allows a definite recognition of the spot.<sup>19</sup> Another approach uses a spatial light modulation array to switch the subapertures on and off so as to allow the spots to enter the adjacent subapertures.<sup>20</sup>

J. Lee (junwon.lee@kodak.com) is with the Display Science and Technology Center, Eastman Kodak Company, 1700 Dewey Avenue, Rochester, New York 14650. R. V. Shack and M. R. Descour are with the Optical Sciences Center, University of Arizona, 1630 East University Boulevard, Tucson, Arizona 85721.

Received 2 February 2005; revised manuscript received 18 March 2005; accepted 24 March 2005.

0003-6935/05/234838-08\$15.00/0

© 2005 Optical Society of America

In this paper we present a simple and robust technique for extending the dynamic range by using software rather than hardware. Software-based solutions are faster than hardware-based solutions and do not require extra cost.<sup>18</sup> The technique that we present in this paper requires only the sorting of focal spots in a special sequence that is based on the  $x$  and  $y$  position of the centroid of the focal spots. So we call it the sorting method. The simplicity and robustness of the sorting method result from the unique characteristics of the Shack–Hartmann sensor, that is, the linear algebraic relationship between focal-spot displacements and the wave-front slope. It is well known that the process of wave-front reconstruction is equivalent to solving these linear algebraic equations. In principle the sorting method requires that the linear algebraic equations be sorted in a certain sequence. For example, this paper uses singular value decomposition (SVD) to solve the linear algebraic equations.<sup>12,14</sup> The SVD requires a precalculated sensitivity matrix whose rows correspond to displacement of the focal spots. The essence of the sorting method is to sort the rows in a predetermined sequence. Theoretical details are presented in Section 2.

In Section 2 we review the principle of the Shack–Hartmann wave-front sensor and describe the theoretical development of the sorting method. Although the principle of the Shack–Hartmann wave-front sensor is well known, it is necessary to revisit it to develop the sorting method. In Section 2 we also discuss the limitations of the conventional and sorting methods. We present the calculation example where the maximum wave front can be measured by using two methods. In Section 3 we present an experimental example of the sorting method to show the extension of the dynamic range. The unconventional optics is measured, and its wave front is reconstructed with the sorting method. We also introduce an actual Shack–Hartmann wave-front sensor built for implementing the sorting method in Section 4.

## 2. Mathematical Background of the Sorting Method

Basically the Shack–Hartmann wave-front sensor is designed to measure the displacement of focal spots. Among several possible ways to detect displacement we chose to calculate a shift in the center of gravity or centroid. It can be shown that displacement of a centroid or spot displacement ( $\Delta x_j$ ,  $\Delta y_j$ ) is linearly proportional to the average local slope of the incident wave front across a single lenslet<sup>21</sup>:

$$\begin{aligned}\Delta x_j &= -\frac{f}{A} \int_{A_j} \frac{\partial W(x, y)}{\partial x} dx dy, \\ \Delta y_j &= -\frac{f}{A} \int_{A_j} \frac{\partial W(x, y)}{\partial y} dx dy,\end{aligned}\quad (1)$$

where  $f$  and  $A$  represent the focal length and the

two-dimensional size of the lenslet, respectively;  $W(x, y)$  is an incident wave front; and  $A_j$  is the area of the  $j$ th lenslet and is called a subaperture. Notice that the slope of the wave front is averaged over the subaperture.

Among several ways to reconstruct the wave front the modal estimation is most popularly used.<sup>9</sup> The modal estimation requires decomposition of the wave front with a set of basis functions. The wave-front construction is equivalent to the estimation of coefficients of each basis function. Let us assume a wave front  $W(x, y)$  decomposed with some basis functions  $\{B_i(x, y)\}$ :

$$W(x, y) = \sum_{i=1}^{i_{\max}} c_i B_i(x, y), \quad (2)$$

where  $B_i(x, y)$  is the  $i$ th basis function,  $c_i$  is its coefficient, and  $i_{\max}$  is an expansion truncation number. The sorting method puts no constraint on selection of the basis polynomial. In Section 3 the Zernike polynomial is chosen to demonstrate the sorting method. By plugging Eq. (2) into Eq. (1), we obtain two linear equations per focal spot:

$$\begin{aligned}\Delta x_j &= -\frac{f}{A_j} \int_{A_j} \frac{\partial \left[ \sum_{i=1}^{i_{\max}} c_i B_i(x, y) \right]}{\partial x} dx dy \\ &= \sum_{i=1}^{i_{\max}} \left[ -\frac{f}{A_j} \int_{A_j} \frac{\partial B_i(x, y)}{\partial x} dx dy \right] c_i, \\ \Delta y_j &= \sum_{i=1}^{i_{\max}} \left[ -\frac{f}{A_j} \int_{A_j} \frac{\partial B_i(x, y)}{\partial y} dx dy \right] c_i.\end{aligned}\quad (3)$$

If there are  $N$  focal spots, there are  $2 \times N$  equations with  $i_{\max}$  of unknown coefficients. For simplicity Eqs. (3) can be represented in matrix notation:

$$\Delta = S \cdot \mathbf{c}, \quad (4)$$

where  $\Delta$  contains  $x$ - and  $y$ -spot displacement data and is a  $2N \times 1$  column vector. The column vector  $\mathbf{c}$  contains  $i_{\max}$  of unknown coefficients. The matrix  $S$  is called the sensitivity matrix. By solving Eq. (4) for an unknown vector  $\mathbf{c}$ , the wave front is reconstructed. We select the SVD to solve Eq. (4) because the SVD is robust<sup>18</sup> and available in many commercial software packages. The SVD is used to calculate a pseudoinverse matrix to solve Eq. (4) in a least-squares sense.<sup>14</sup> The solution is

$$\hat{\mathbf{c}} = S^+ \cdot \Delta, \quad (5)$$

where  $S^+$  is a pseudoinverse matrix of the sensitivity matrix and  $\hat{\mathbf{c}}$  is a least-squares-sense solution. Note that the rows in the sensitivity matrix correspond to the spot displacements, and their sequence has no

effect on wave-front reconstruction. The sorting method generates a special sequence of spot displacements that allow the expansion of the dynamic range without affecting wave-front reconstruction.

In a conventional Shack–Hartmann wave-front sensor the dynamic range is limited by the  $f$ -number of the lenslet. A spot is required to stay inside a subaperture defined by the original lenslet. If a wave front varies so fast that a spot displacement goes beyond the subaperture, a spot cannot be assigned to the original lenslet and the reference focal spot. The spot displacement cannot be determined without knowing the reference position. From Eq. (1) the maximum wave-front slope is expressed as

$$\left| \frac{1}{A} \int_{A_j} \left[ \frac{\partial W(x, y)}{\partial x} \right] dx dy \right| = \frac{w}{2f},$$

$$\left| \frac{1}{A} \int_{A_j} \left[ \frac{\partial W(x, y)}{\partial y} \right] dx dy \right| = \frac{w}{2f}, \quad (6)$$

where  $w$  is the width of the subaperture.

The key issue is how to assign the correct reference positions to the focal spots even if they leave their original subaperture. We call the focal spots generated by an aberrated wave front aberrated focal spots or simply aberrated spots. The reference position can be the center of the corresponding lenslet or the reference focal spot created by a planar wave front. The latter is a better choice because the mechanical error or the aberration of the components can be compensated. Usually the reference focal spot is measured only once and saved for future use.

The sorting process assigns the correct reference focal spots to the aberrated spots by sorting the reference focal spots and the aberrated focal spots in the same sequence. Figure 1 shows a sample set of reference spots and the corresponding aberrated spots before the sorting process. The rectangular grids indicate the subapertures that are projected on the image plane where the focal spots are formed. Let us assume that the position of the focal spots is from one known universal origin. This is possible because the intensity of the focal spot is recorded on an integrated digitization sensor such as a CCD chip. The O in the left lower corner is chosen as the universal origin in our case. The position data are represented by the Greek characters in Fig. 1. As shown in Fig. 1, bottom, the aberrated spots have already exceeded the conventional limit of the dynamic range. From the reference spots one can determine how many spots there are in each row in the region of interest. For example, the first five lowest spots belong to the lowest row (row 1), and the next seven lowest spots belong to the second lowest row (row 2). The same idea is applied to the aberrated focal spots. To determine which rows each spot belongs to, the aberrated spots in Fig. 1, bottom, should be sorted by their  $y$  position. Figure 2 shows the sorting result, and the focal spots are tagged with the row number.

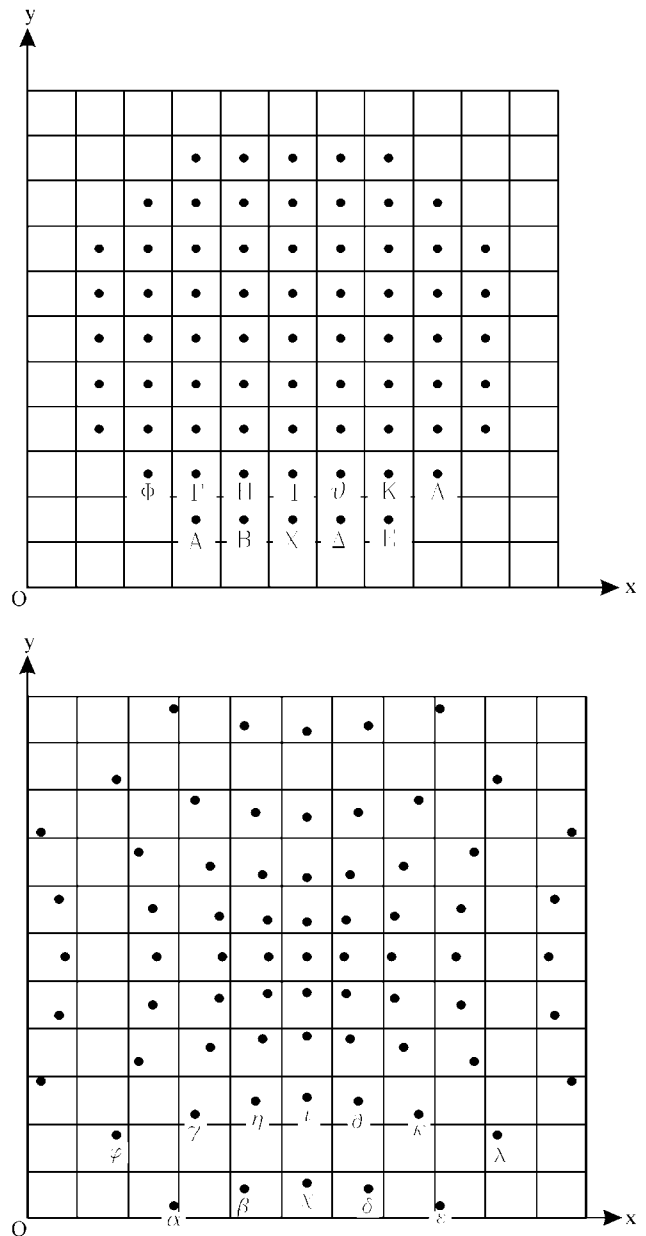


Fig. 1. Plot of the focal spots before sorting is performed: top, reference focal spots; bottom, aberrated focal spots in the same configuration as in the top figure. The rectangular grid indicates the subaperture bounded by the lenslet array.

The  $\alpha_1$  means that the focal spot  $\alpha$  belongs to the first row, that is, the lowest row. We select the five lowest spots ( $\alpha_1, \beta_1, \gamma_1, \delta_1, \varepsilon_1$  in Fig. 2) according to their  $y$  position and let them belong to the lowest row. The same procedure can be repeated for the rest of the focal spots. Every focal spot is tagged with a row number.

After sorting by the  $y$  position, we sort the focal spots in each row by the  $x$  position; the result is in Fig. 3. Unlike the previous sorting where every focal spot is considered in the region of interest simultaneously, in sorting by the  $x$  position we consider only the focal spots belonging to a single row. The  $x$ -position sequence is tagged after the row number. For example,

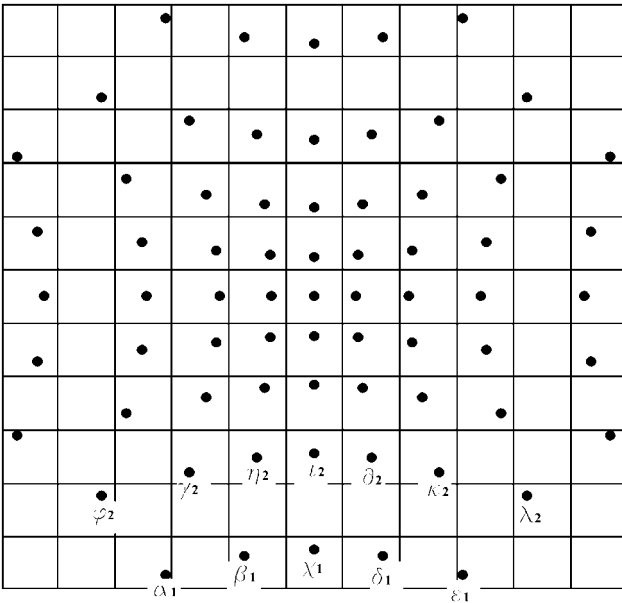


Fig. 2. Plot of aberrated focal spots after sorting is performed in the  $y$  position.

$\chi_{1,3}$  means that focal spot  $\chi$  belongs to the first row, and its  $x$ -position sequence in the first row is third. The positions of the focal spots in the first row are saved in the column vector with the sequence determined by the sorting procedure, that is,

$$(\mathbf{p}_a)^T = \{\alpha_{1,1}, \beta_{1,2}, \chi_{1,3}, \delta_{1,4}, \epsilon_{1,5}\}, \quad (7)$$

where  $\mathbf{p}_a$  is termed the centroid position vector for the aberrated focal spots and  $T$  is a transpose operator. We can apply the same procedure for the next seven spots in the second lowest row and append those to

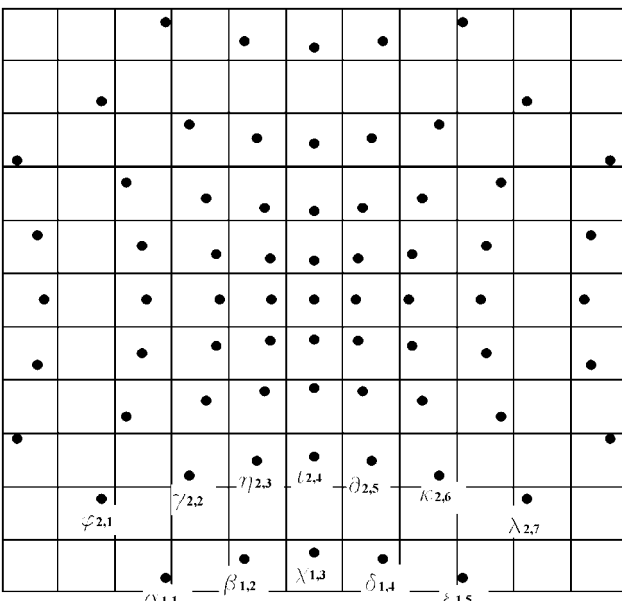


Fig. 3. Plot of aberrated focal spots after sorting is performed in the  $y$  and  $x$  positions sequentially.

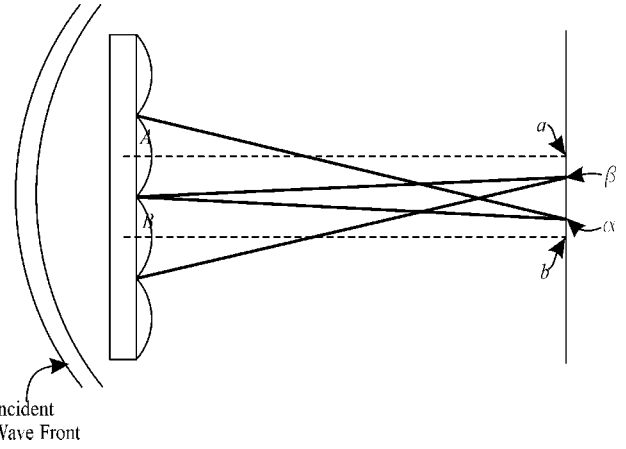


Fig. 4. Spot crossing. Two adjacent focal spots cross each other.

the first five spot data in the centroid position vector, that is,

$$(\mathbf{p}_a)^T = \{\alpha_{1,1}, \beta_{1,2}, \chi_{1,3}, \dots, \varphi_{2,1}, \psi_{2,2}, \eta_{2,3}, \dots\}. \quad (8)$$

The procedure is repeated until every spot is sorted. Note that the spots are sequenced not by subaperture location but by their centroid positions. The same steps can be applied to the reference spots to create a centroid position vector  $\mathbf{p}_r$ .

$$(\mathbf{p}_r)^T = \{A_{1,1}, B_{1,2}, X_{1,3}, \dots, \Phi_{2,1}, \Gamma_{2,2}, H_{2,3}, \dots\}. \quad (9)$$

Since the sequence of two centroid position vectors is the same, the spot displacement can be calculated correctly by subtracting two vectors:

$$\mathbf{p}_a - \mathbf{p}_r = \Delta. \quad (10)$$

It is valid even if the aberrated focal spots leave their original subapertures as shown in Fig. 3. There are a few occasions in which the sorting method fails. They are discussed in Section 3. The remaining step is to reconstruct the wave front by using Eq. (5) and the precalculated sensitivity matrix.

### 3. Expansion of the Dynamic Range

In this section we address the expansion of the dynamic range by the sorting method. The sorting method is limited by two types of focal spot crossing. One is a crossing between adjacent spots and is called spot crossing. The other is a crossing between adjacent rows and is called row crossing. Spot crossing occurs when two adjacent focal spots overlap or cross owing to the fast-varying wave-front slope. One example is illustrated in Fig. 4. Let us assume that one lenslet  $A$  has optic axis (or reference position)  $a$  and the other lenslet  $B$  has optic axis  $b$ . Since the incident wave front varies fast over the two lenslets, the upper lenslet  $A$  creates focal spot  $\alpha$  below focal spot  $\beta$  cre-

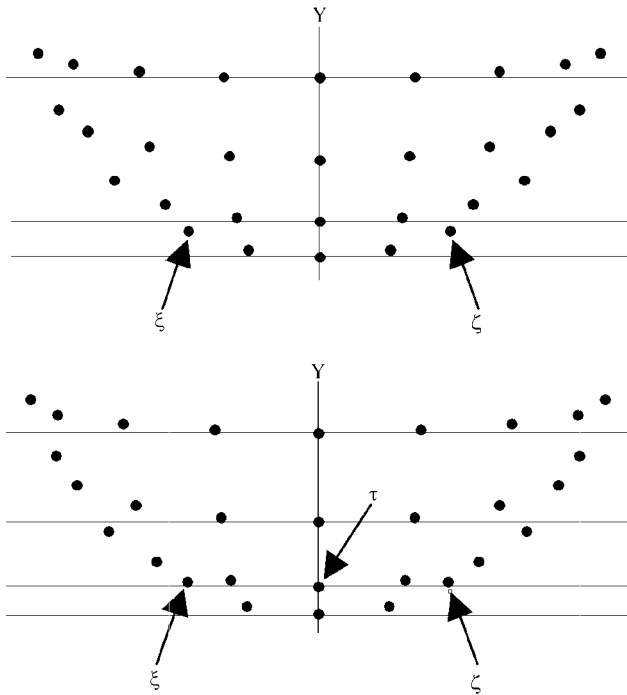


Fig. 5. Row crossing. Horizontal lines pass on the spots that are aligned on the  $y$  axis: top, spot displacement when the wave front has  $24\lambda$  of spherical aberration; bottom, crossing of two adjacent rows when the wave front has  $27\lambda$  of a spherical aberration.

ated by lower lenslet  $B$ . The sorting method assigns reference position  $a$  to the aberrated spot  $\beta$  and vice versa so that it calculates an incorrect spot displacement. Mathematically the spot crossing starts when variation of the wave front over two adjacent lenslets is

$$\frac{1}{w \cdot A} \left\{ \int_{A_j} \left[ \frac{\partial W(x, y)}{\partial x} \right] dx dy - \int_{A_{j \pm 1}} \left[ \frac{\partial W(x, y)}{\partial x} \right] dx dy \right\} = \frac{1}{f}. \quad (11)$$

It is not difficult to notice that in Eq. (11) the variation in the averaged wave-front slope is calculated over two adjacent lenslets, which corresponds to the curvature of the wave front. In other words the sorting method is generally limited not by the slope of the wave front but by the curvature of wavefront. Compared with Eqs. (6), Eq. (11) indicates that the sorting method results in a much larger dynamic range. For example, let us assume that the image of the exit pupil has a diameter of 2.7 mm, the lenslet's focal length is 7.8 mm, and its aperture width is 0.3 mm. Spot crossing would occur when the wave-front curvature has 70 waves of defocus over the entire exit pupil. According to Eq. (6) the conventional method can measure as many as nine waves of defocus in the same conditions.

Row crossing is illustrated in Fig. 5. The spot displacements are created by  $24\lambda$  of spherical aberration in Fig. 5, top, and  $27\lambda$  of spherical aberration in Fig. 5, bottom. The two spots,  $\xi$  and  $\zeta$ , are the highest spots in the first row, and  $\tau$  is the lowest spot in the second row. The two spots,  $\xi$  and  $\zeta$ , start moving up as the spherical aberration increases. In Fig. 5, bottom,  $\xi$  and  $\zeta$  are located higher than  $\tau$  so that the sorting by the  $y$  position would fail to count the first five spots correctly. Based on this phenomenon, the maximum measurable wave front is determined by

$$\max \left\{ \frac{1}{w \cdot A} \left| \int_{A_j} \left[ \frac{\partial W(x, y)}{\partial y} \right] dx dy - \int_{A_k} \left[ \frac{\partial W(x, y)}{\partial y} \right] dx dy \right| \right\} = \frac{1}{f}, \quad (12)$$

where  $A_j$  and  $A_k$  are the two-dimensional range of any subaperture in two adjacent rows.

Zernike polynomials may be used to calculate the dynamic-range expansion afforded by our sorting method. In Table 1 we report the maximum Zernike coefficients that can be measured for a particular example by two different methods: a conventional

Table 1. Calculation of the Maximum Zernike Coefficient in Waves<sup>a</sup>

Zernike Coefficients	Name	Conventional Method	Sorting Method
$Z_3$	Defocus	19.16	328.04
$Z_4$	Astigmatism along the $x$ axis	38.32	656.09
$Z_5$	Astigmatism along the $y$ axis	38.32	656.09
$Z_6$	Coma along the $x$ axis	11.37	46.65
$Z_7$	Coma along the $y$ axis	11.37	46.65
$Z_8$	Primary spherical	6.49	19.09
$Z_9$	Trefoil $x$ axis	26.82	50.1
$Z_{10}$	Trefoil $y$ axis	26.82	50.1
$Z_{11}$	Secondary astigmatism along the $x$ axis	8.96	45.94
$Z_{12}$	Secondary astigmatism along the $y$ axis	8.96	45.94
$Z_{13}$	Secondary coma along the $x$ axis	4.79	11.73
$Z_{14}$	Secondary coma along the $y$ axis	4.79	11.73
$Z_{15}$	Secondary spherical	3.28	6.83

<sup>a</sup>The exit pupil has a radius of 3.15 mm.

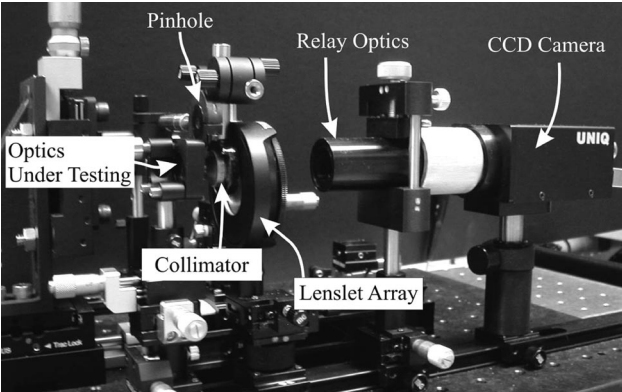


Fig. 6. Actual Shack–Hartmann wave-front sensor. The pinhole is moved out of sight. The system total track is 15 cm, which is the distance from the optics being tested to the CCD chip.

method whose dynamic range is limited by Eq. (6) and a sorting method whose dynamic range is limited by Eqs. (11) and (12). The sequence and name of the Zernike polynomials follow the University of Arizona rule.<sup>22</sup> The exit pupil in these calculations has a radius of 3.15 mm. The lenslet's focal length is 7.8 mm, and its aperture width is 0.3 mm. As seen in Table 1 the dynamic range increased by a factor of 17 in the low-order Zernike polynomials. The extension of the dynamic range is reduced at high Zernike polynomials because the sorting method is limited by the wave-front curvature and works best with the Zernike polynomials that have second-order dependence such as  $Z_3$ ,  $Z_4$ , and  $Z_5$ .

#### 4. Experimental Demonstration

The most critical part of this paper is demonstration of the sorting method in a real measurement procedure. We built a Shack–Hartmann wave-front sensor to implement the sorting method experimentally (see Fig. 6). The main parts of the Shack–Hartmann wave-front sensor include a collimator, lenslet array, pinhole, relay optics, and CCD camera. It is noticeable that the pinhole (Melles Griot, 04PPM001) is inserted between the optics under testing and the collimator to create a reference wave front, namely, a spherical wave front. Its diameter is 2  $\mu\text{m}$ , which can create a spherical wave front as large as 0.6 of N.A.<sup>23</sup> It will be removed when the test wave front is measured.

We chose a rectangular lenslet array (Adaptive Optics Associates, 0300-7.6-S) whose focal length is 7.6 mm and size is 0.3 mm  $\times$  0.3 mm. The CCD camera (Uniq Vision, UP 1800) is located at the back focal plane of the lenslet array. Its pixel size is 6.45  $\mu\text{m}$ , and the number of pixels is 1392  $\times$  1040. The relay optics (Edmund Industrial Optics, NT45-759) between the lenslet array and the CCD camera relays focal spots onto the CCD camera. It has a unit magnification and diffraction-limited performance over the entire field of view. It is not necessary that the  $f$ -number of the lenslet be large enough to let the focal spots reach the CCD camera.

The optics under test is a cubic phase plate from CDM Optics.<sup>24</sup> We chose this unconventional and nonrotationally symmetric optical element to demonstrate the versatility of the sorting method. It creates a highly aberrated wave front sufficient for observing the focal spots leaving the original subapertures. The cubic phase plate creates a phase delay that has a cubic dependence on the  $x$  and  $y$  positions. The phase delay is

$$P(x, y) \propto \frac{2\pi}{\lambda} (x^3 + y^3). \quad (13)$$

Note that the phase delay is equivalent to the wave front behind the cubic phase plate if a planar wave front is incident on the cubic phase plate. Before the cubic phase plate is mounted, reference focal spots are measured by sending a plane wave front without the optics being tested. The same procedure is repeated after the cubic phase plate is mounted. Since the reference focal spots are recorded only once, the sorting method is different from the approach requiring measurements of the focal spots at multiple positions. Figure 7 shows the measured spot displacements that are the result of the subtraction of the reference focal spots, the aberrated focal spots, and the corresponding reconstructed wave front. The patterns in Fig. 7 show the unique characteristics of a cubic phase plate (see the point-spread function and phase plot in Ref. 25). Note that the maximum spot displacement is 0.33 mm in Fig. 7, top. This is twice as large as the dynamic range of the conventional method, which is 0.15 mm. The sorting method succeeds in reconstructing the wave front with focal spots whose displacement exceeds the conventional limitation.

#### 5. Conclusion

We have introduced a new approach for extending the dynamic range of the Shack–Hartmann wave-front sensor by using software. The sorting method is a software-based solution that can be implemented more easily than a hardware-based solution. It overcomes the dynamic-range limitation of the conventional Shack–Hartmann wave-front sensor by sorting each spot in a special sequence. Its mathematical development is presented in Section 2. There are two situations that limit the sorting method: the spot crossing and the row crossing. They are addressed in Section 3 and used to calculate the maximum dynamic-range expansion in several examples. In Section 4 we demonstrate the capability of the sorting method through the actual wave-front measurement. The sorting method reconstructs the highly aberrated wave front and exceeds the dynamic range of the conventional Shack–Hartmann wave-front sensor. The optics being tested creates a wave front that is nonrotationally symmetric and highly aberrated. This demonstration indicates the imminent application of the sorting method: the highly aberrated

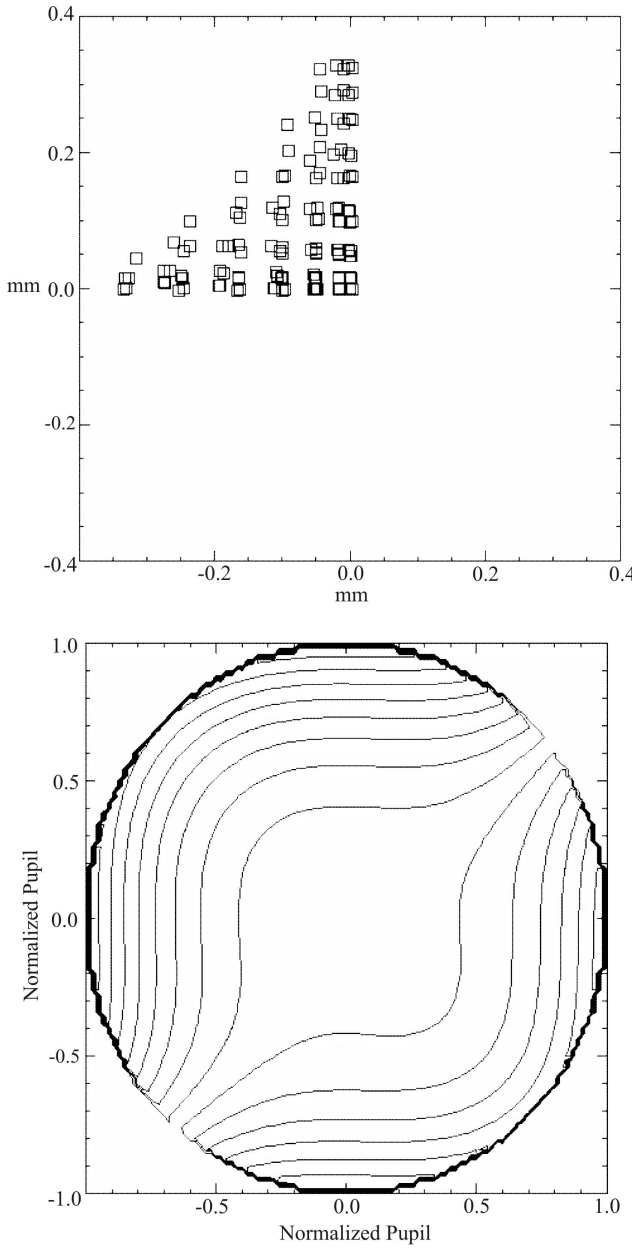


Fig. 7. Spot displacements and the reconstructed wave front of a cubic phase plate. The patterns show the unique characteristics of the cubic phase plate.

wave-front measurement of unconventional optics that has become more popular nowadays.

It has been found that the sorting method is generally limited by the wave-front curvature in the mathematical development. This fact is confirmed in the calculation example that shows that the sorting method performs best in a low-order Zernike polynomial. The Shack–Hartmann wave-front sensor built for the demonstration has neither a special configuration nor an extra component. It is evident that the sorting method can be easily adapted to any generic Shack–Hartmann wave-front sensor by using a rectangular lenslet array.

The main advantages of the sorting method are

its simplicity and robustness. We have described the sorting method algorithm and quantified its dynamic-range expansion. Because of these advantages, it may be successfully applied to the testing of uncommon and highly aspherical optics under the limitation of the crossing with minimum cost.

We acknowledge help from Thomas Cathey and CDM Optics. We also thank David Kessler, Eastman Kodak Company, and John E. Greivenkamp, University of Arizona, for thoughtful comments.

This research was supported by grants from the National Science Foundation, ECS-0074578 and BES-0086736, and the National Cancer Institute, CA091454.

## References

- B. C. Platt and R. Shack, "History and principles of Shack–Hartmann wave-front sensing," *J. Refract. Surg.* **17**, s573–s577 (2001).
- I. Ghozeil, "Hartmann and other screen tests," in *Optical Shop Testing*, D. Malacara, ed., Wiley Series in Pure and Applied Optics (Wiley, 1992), pp. 367–396.
- J. W. Hardy, "Adaptive optics: a new technology for the control of light," *Proc. IEEE* **66**, 651–697 (1978).
- C. J. Solomon, J. C. Dainty, and N. J. Woorder, "Bayesian estimation of atmospherically distorted wave fronts using Shack–Hartmann sensor," *Opt. Rev.* **2**, 217–220 (1995).
- J. Liang, B. Grimm, S. Goetzl, and J. F. Bille, "Objective measurement of wave aberrations of the human eye with the use of a Hartmann–Shack wave-front sensor," *J. Opt. Soc. Am. A* **11**, 1949–1957 (1994).
- J. Liang and D. R. Williams, "Aberrations and retinal image quality of the normal human eye," *J. Opt. Soc. Am. A* **14**, 2873–2883 (1997).
- D. L. Fried, "Least-square fitting a wave-front distortion estimate to an array of phase-difference measurements," *J. Opt. Soc. Am.* **67**, 360–369 (1977).
- R. J. Noll, "Phase estimates from slope-type wave-front sensors," *J. Opt. Soc. Am.* **68**, 139–140 (1978).
- W. H. Southwell, "Wave-front estimation from wave-front slope measurement," *J. Opt. Soc. Am.* **70**, 998–1006 (1980).
- J. Hermann, "Least-squares wave-front errors of minimum norm," *J. Opt. Soc. Am.* **70**, 28–35 (1980).
- G. H. Golub and C. F. van Loan, *Matrix Computations*, 2nd ed. (Johns Hopkins U. Press, 1989), Chap. 2, pp. 48–86.
- W. H. Press, S. A. Teukolsky, W. T. Vetterling, and B. P. Flannery, *Numerical Recipe in C++*, 2nd ed. (Cambridge U. Press, 1993), Chap. 2, pp. 35–107.
- Å. Björk, *Numerical Methods for Least Squares Problems*, 1st ed. (Society for Industrial and Applied Mathematics, 1996), Chap. 1, pp. 1–36.
- H. H. Barrett and K. J. Myers, *Foundations of Image Science*, 1st ed. (Wiley, 2003), Chap. 1, pp. 1–62.
- J. Pfund, N. Lindlein, and J. Schwider, "Dynamic range expansion of a Shack–Hartmann sensor by using a modified unwrapping algorithm," *Opt. Lett.* **23**, 995–997 (1998).
- T. L. Bruno, A. Wirth, and A. J. Jankevics, "Applying Hartmann wavefront-sensing technology to precision optical testing of the HST correctors," in *Active and Adaptive Optical Components and Systems II*, M. A. Ealey, ed., Proc. SPIE **1920**, 328–336 (1993).
- M. C. Roggermann and T. J. Schulz, "Algorithm to increase the largest aberration that can be reconstructed from Hartmann sensor measurements," *Appl. Opt.* **37**, 4321–4329 (1998).
- S. Groening, B. Sick, K. Donner, J. Pfund, N. Lindlein, and J.

- Schwider, "Wave-front reconstruction with a Shack-Hartmann sensor with an iterative spline fitting method," *Appl. Opt.* **39**, 561–567 (2000).
19. N. Lindlein, J. Pfund, and J. Schwider, "Expansion of the dynamic range of a Shack-Hartmann sensor by using astigmatic microlenses," *Opt. Eng.* **39**, 2220–2225 (2000).
20. N. Lindlein, J. Pfund, and J. Schwider, "Algorithm for expanding the dynamic range of a Shack-Hartmann sensor by using a spatial light modulator array," *Opt. Eng.* **40**, 837–840 (2001).
21. G. Rousset, "Wave-front sensing," in *Adaptive Optics for Astronomy*, D. M. Alloin and J.-M. Mariotti, eds., Vol. 423 of NATO Advanced Science Institutes Series (Kluwer Academic, 1994), pp. 115–138.
22. J. C. Wyant, "Zernike polynomial," Optical Science Center, University of Arizona, Tucson, Arizona, 1999, <http://www.optics.arizona.edu/jcwyant/Zernikes/ZernikePolynomials.htm>.
23. G. E. Sommargren, "Phase shifting diffraction interferometry for measuring extreme ultraviolet optics," in *Extreme Ultraviolet Lithography*, G. D. Kubiak and D. R. Kania, eds., Vol. 4 of OSA Trends in Optics and Photonics Series (Optical Society of America, Washington, D.C., 1996), pp. 108–112.
24. CDM Optics, Inc., Suite 2110, 4001 Discovery Drive, Boulder, Colo. 80303, <http://www.cdm-optics.com>.
25. E. R. Dowski and W. T. Cathey, "Extended depth of field through wave-front coding," *Appl. Opt.* **34**, 1859–1866 (1995).